Atmospheric Environment 266 (2021) 118740

Contents lists available at ScienceDirect

Atmospheric Environment

journal homepage: www.elsevier.com/locate/atmosenv

Distinguishing in-cloud and below-cloud short and distal N-sources from high-temporal resolution seasonal nitrate and ammonium deposition in Vienna, Austria

Lucilena R. Monteiro [1,*], Stefan Terzer-Wassmuth, Ioannis Matiatos, Cedric Douence, Leonard I. Wassenaar

Isotope Hydrology Section, Division of Physical and Chemical Sciences, Department of Nuclear Sciences and Applications, International Atomic Energy Agency, Vienna International Centre, A-1400, Vienna, Austria

HIGHLIGHTS

- Excess reactive nitrogen (N_r) in precipitation is a major global air pollutant.
- N_r in Vienna precipitation events were investigated in hourly in wet deposition for a year.
- N_r was controlled by local motor traffic and by distal sources associated with rainout processes.
- HYSPLIT analysis revealed that N_r sources coincided with well-known NOx hotspots in Europe.

GRAPHICAL ABSTRACT

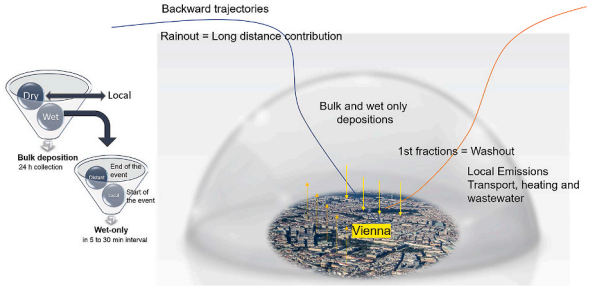

ARTICLE INFO

Keywords:
Rainout
Washout
Scavenging ratio
Nitrogen pollution
High-resolution sampling

ABSTRACT

Reactive nitrogen (N_r: nitrate and ammonium) washout in Vienna (Austria) precipitation events were investigated in 2019. A total of 958 samples from 61 rain events representing >90% of annual precipitation were collected at 5–30 min intervals for nitrate (NO_3^-) and ammonium (NH_4^+) analyses and meteorological information. The data revealed systematic seasonal concentration variations for all N_r-species and a clear influence of rush-hour traffic on the kinetics of N-scavenging processes. The monthly nitrate and ammonium deposition was 0.69 ± 0.21 kg ha^{-1} month^{-1} and 1.02 ± 0.30 kg ha^{-1} month^{-1}, respectively. Around 30% of nitrate and 20% of ammonium was dry deposition, and ~30% of each N-species was from distal sources associated with rainout processes. The half-life of below-cloud N-species were similar in the warmer seasons (1.7 ± 0.2 h and 2.3 ± 0.4 h for nitrate and ammonium). In winter, the ammonium half-life was significantly lower (1.4 h). N_r removal by wet-only in-cloud scavenging was slower than predicted by empirical models. HYSPLIT trajectory analysis revealed that N_r rainout from distal sources in spring had no prevailing direction, but higher N_r contributions

* Corresponding author.
E-mail addresses: l.monteiro@iaea.org, luciremo@uol.com.br (L.R. Monteiro).
[1] now at Ipen - Instituto de Pesquisas Energéticas e Nucleares Av. Lineu Prestes 2242 - Cidade Universitária - CEP: 05508-000 - São Paulo - SP BRAZIL (lrmonteiro@ipen.br).

https://doi.org/10.1016/j.atmosenv.2021.118740
Received 8 June 2021; Received in revised form 7 September 2021; Accepted 19 September 2021
Available online 23 September 2021

were from N and W. In summer and winter, air masses from W, SW and SE were related to intense, medium, and low N_r contributions, respectively. The origin and path of these trajectories coincided with known NO_x hotspots in Europe.

1. Introduction

The steady rise of excess anthropogenic reactive nitrogen (N_r) and its and impacts on the environment (e.g. acid rain, water pollution), human health, and corresponding economic impacts is a major global concern, and particularly for highly industrialized parts of the world (Feng et al., 2021; Malagó and Bouraoui, 2021; Reis et al., 2009). This has led to various policy regulations regarding air and water quality at regional and national scales with the goal to reduce overall N emissions to air and water (UNEP, 2007). Reactive nitrogen deposition (N_r; NO_3^- and NH_4^+) has been studied in highly urbanized areas (Li et al, 2016, 2020, 2016; Stevenazzi et al., 2020; Ye et al., 2019), industrialized regions (Porfírio et al., 2020; Xiao, 2016), and in remote or pristine areas (Bhattarai et al., 2019; Holtgrieve et al., 2011; Keene et al., 2015; Zhang et al., 2017).

Wet deposition is the predominant sink of N_r from anthropogenic aerosols and an important pathway for nitrogen and other teleconnected contaminant contributions to terrestrial and aquatic ecosystems. Therefore, a better understanding of wet deposition N dynamics is essential to assess air pollutant dispersion at global level (Malagó and Bouraoui, 2021; Vet et al., 2014). Consequently, continuous long-term monitoring records for N_r species are available for some countries (Cheng and Zhang, 2016; Feng et al., 2021; Roy et al., 2019; Wen et al., 2020). In Austria, N_r monitoring is done by the Federal Environment Agency – Umweltbundesamt (Leder et al., 2003; H. Puxbaum et al., 2002; Smidt, 2008, 2007), to model the atmospheric deposition of N and other pollutants (Vizcaino and Lavalle, 2018) and to improve predictive air quality multivariate models (European Environment Agency, 2021). However, scavenging through wet deposition is currently assessed by comparing concentrations of N_r species against source variables, such as land use, traffic patterns and physical environmental variables as the predictors. Often, local, and distal N_r contributions are mixed and daily or event-based sampling. Therefore, the 24 h or event-based sampling performed in most of the precipitation monitoring stations do not allow for N_r source identification (See Figure S1 in the supplementary material). So far, most studies use integrated daily events by aggregating 24 h to 2 weeks' time spans of precipitation events. In most studies, high frequency sequential sampling is difficult and restricted to short periods of few weeks at a time (Aikawa et al., 2014; Aikawa and Hiraki, 2009; Celle-Jeanton et al., 2009a; Karadeniz and Yenisoy-Karakaş, 2020). In the absence of high-frequency measurements of local data, these studies need to apply empirical estimates of residence times based on other radionuclides (Sportisse, 2007) or different chemical species under the assumption that most N pollutants behave similarly (Sportisse and Bois, 2002). By using high-frequency precipitation collections, the event evolution and the N_r deposition kinetics can be observed and more effectively modeled. Kinetic modeling allows for estimation of the scavenging coefficients (SCs), a variable that explains where and how fast these chemical species are removed from the atmosphere (Ervens, 2015).

In urbanized environments, fossil fuel emissions (vehicular traffic and power generation) and other industrial activities are the primary sources of below-cloud N-deposition. Conversely, emissions from natural N-sources stem from natural and agricultural soil emissions or lightning and are linked to in-cloud formation processes after long-distance advection (Lee et al., 2000). Therefore, enabling a clear distinction between local versus distal N sources, or anthropogenic versus natural N_r contributions is important but complex (Chen et al., 2017). Some studies use stable isotopes, particularly ^{15}N and ^{18}O of NO_3^- and NH_4^+ that have proven useful (Beyn et al., 2014; Ciężka et al., 2016; Villalobos-Forbes et al., 2021). Regarding the 2019 Vienna precipitation events, the use of stable isotopes to identify the source apportionment is underway separately (Matiatos et al., 2021). Considering the chemical components, many studies focus on the major and minor ion concentrations to characterize local conditions and to detect changes between rain events (Celle-Jeanton et al., 2009b; Xiao, 2016). However, the balance between in-cloud and below-cloud contributions gives valuable insight on wet deposition removal processes, relevant to atmospheric chemistry, air quality and climate studies (Gong et al., 2003; Laakso et al., 2003; Tost et al., 2006). The distinction between rainout (in-cloud) and washout (below-cloud) is key to understand how fast and efficient the sink of N_r species occur. The large variability in precipitation sources and N_r concentrations mandates a higher temporal (intra-event) sampling resolution on a seasonal basis (Montoya-Mayor et al., 2011; Spanos et al., 2002). One recommended approach to quantify N_r washout/rainout contributions uses 0.5–1 mm rainfall collection steps within each precipitation event (Aikawa and Hiraki, 2009). However, such assessments are seldomly performed at the high temporal resolution needed over year-long or seasonal sampling campaigns.

Here we present results from a high frequency sampling covering >90% precipitation across all seasons for Vienna. This experimental design allowed us to obtain estimates of the rainout and washout fractions of N_r species and better (a) disentangle local and distal N_r fractions and (b) assess the SC of N_r species that describe its removal from the air. The sampling was complemented by comparative conventional 24 h integrated collections and meteorological recordings and air mass back trajectory analysis. Our findings help to improve NO_x and NH_x emission/deposition inventories and spatiotemporal atmospheric dispersion models as well as validation of remote sensing measurements of the air gas column that assist the study of global pollutant transport models (Schreier et al., 2020).

2. Material and methods

2.1. Study area

Rainwater sampling and meteorological monitoring was conducted at a metropolitan study site in the city of Vienna (Austria) at the Vienna International Centre (VIC, Fig. 1). The site was a rooftop station at 48° 14′ 10″ N 16° 24' 57" E at an elevation of ca. 170 meters. The predominant wind direction was N and NE during day and night seasonal sampling. The highest wind speeds were from the S in all seasons except for summer when NNE predominated. All seasons but winter exhibited stronger winds during the daytime versus night. Land-use of site surrounding is mainly urban with adjacent motorways and road traffic and a large urban greenspace.

The energy mix in Vienna is considered clean, with contributions from hydroelectric (45.2%) wind (11.6%), biomass (2.8%), solar (1.6%) and other clean energy sources (1.0%) surpassing fossil fuels/gas burning (37.93%) (Wien Energie, 2020). Major point based N_r air pollution sources include three municipal incinerators at 4 km W, 10 km WSW and 7.5 km SE from the sampling site and a municipal wastewater treatment plant with a capacity for three million population volume around 8 km SE (Fig. 1). In 2018, the incinerators produced 5,581 GWh as electrical energy and 4,768 GWh as thermal energy, also 2.734 t of CO_2, 893 t of NO_x, 10 t SO_2 and 3 t of dust were emitted (Wien Energie, 2018). The wastewater treatment plant declared a reference load of 38-tonnes of nitrogen with 70% removal efficiency. A major oil refinery (9.6 Mt a^{-1} crude oil capacity) is located 12 km to the SE.

The metropolitan area of Vienna is 414.9 km^2 with 1.9 million

inhabitants (City of Vienna, 2019). The high traffic hours near the site (distance of 337 m) peak between 7 and 9 am and from 4 p.m. to 8 p.m. (City of Vienna, 2016). Municipal air quality monitoring covers PM_{10}, $PM_{2.5}$, O_3, NO_2, NO_x and SO_2 (Spangl, 2019; Stadt Wien, 2020), with a focus on NO_2 emissions from utility companies (public transportation, communal heating and energy conversion). We used 2018 Vienna air quality data as reference values for below-cloud conditions (City of Vienna, 2019).

2.2.1. Climatology

The reference station for Vienna was the Hohe Warte meteorological observatory (WMO ID 11035) located 4.5 km WNW from the collection site. The climate is temperate and fully humid (Köppen-Geiger type Cfb) with a mean annual precipitation (MAP) of 651 mm slightly biased towards summer (32.5% occur during June to August with a mean annual temperature (MAT) of 10.4 °C for the 1981–2010 reference period (Zentralanstalt für Meteorologie und Geodynamik, 2019). Noteworthy is the microscale distribution of precipitation over Vienna over a W-E gradient with a reference MAP of 516 mm at Groß-Enzersdorf 10.5 km ESE. Assuming a linear gradient, we estimate an average MAP of ca. 610 mm for the site. The year 2019 was exceptionally warm (3rd-warmest on record) with a MAT of 13.0 °C and MAP ranging from 472 to 675 mm, as recorded at Groß-Enzersdorf and Hohe Warte, respectively (Zentralanstalt für Meteorologie und Geodynamik, 2019).

2.2. Site instrumentation

Meteorological information at the site was recorded at 5-min resolution using a Davis Vantage Pro 2 weather station (Davis Instruments, Hayward CA, United States). The tipping-bucket rain gauge had a 0.2 mm resolution. A wet-only automated sequential time-integrated rain collector (Coplen et al., 2015) was used for automated wet-only precipitation sampling by recording initial and final timestamps, air temperature, tipping bucket counts, and ID automatically assigned to each collected sample. By default, the collection intervals were every 15 min from July 2019, after which the programming was modified to accommodate flexible intervals of 5–30 min, or once a minimum of 3 bucket tips were recorded (equaling 0.6 mm of rain or ~ 20 mL sample volume) to better capture intense storm events. The rain sampler returned to a closed-lid sleep mode if no bucket tip was registered for more than 60 min. Not all rain events could be sampled for wet-only precipitation due to small precipitation amounts (the first 0.2 mm of any rain event are lost in the function as the trigger for the autosampler initiation, Coplen et al., 2015). Instead, a rain event bulk sample was collected in these low precipitation events.

The integrated bulk precipitation sampler was custom-made at IAEA and based on the concept of a ball-in-funnel rain sampler (Michelsen et al., 2018). The precipitation collection surface area was 2,500 cm^2. Both samplers were positioned 1.5 m above the roof surface. Bulk sample collection was at 7–9 am daily, with intermediate samplings as needed for synoptic weather or excessive rains. The integrated bulk samples were weighed and filtered through 0.45 μm membranes and stored at 5 °C.

2.3. Precipitation sampling

We collected eighty-one integrated bulk rainwater events (Jan–Dec 2019) and sixty-one wet-only (May–Dec 2019). The precipitation amounts recorded were compared with the meteorological reference stations to assess our sampling coverage. The 61 wet-only events were collected at high-resolution time intervals ranging from 5 to 30 min. The sampler was time- and volume constrained. Sampling was triggered if either the volume reached 20 mL (0.6 mm) or a maximum 30 min interval had elapsed. However, the sample intervals were delayed having multiples of 5 min (the recording interval of our meteorological equipment). A total of 958 fractions of 61 wet-only events were collected for analysis, representing >90% of annual precipitation. The wet-only samples corresponded to ca. 60% of the total precipitation volume

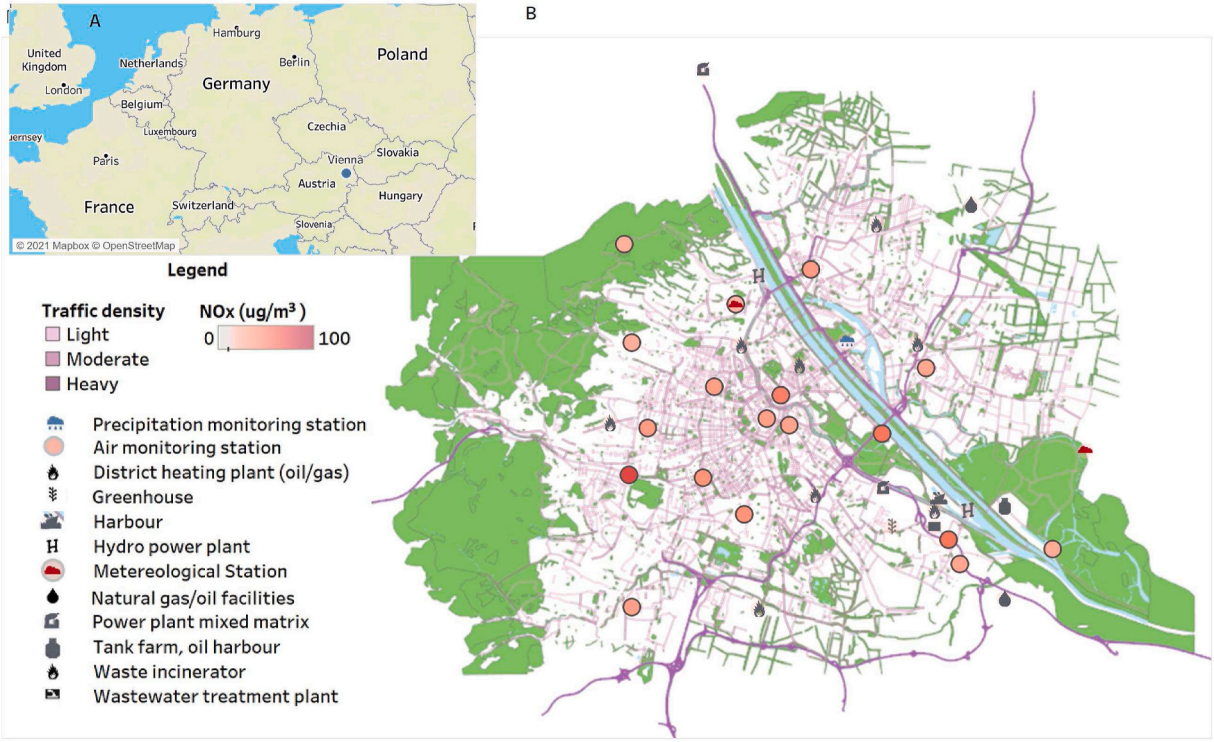

Fig. 1. Precipitation monitoring station (IHL-VIC) including Vienna traffic density (City of Vienna, 2016), air NO_x yearly average (Spangl, 2019), main NO_x point source facilities and green areas (Open Data Österreich, 2020). (For interpretation of the references to color in this figure legend, the reader is referred to the Web version of this article.)

collected by the bulk collector. For most rain events, more than ten sequential wet-only samples were collected, but three intensive precipitation events generated more than forty samples each. The samples remained inside the collector until the end of the event up to 24 h on weekdays and 48 h on weekends.

2.4. Nitrate and ammonia analysis

The high-resolution wet-only samples fraction typically resulted in collection volumes up to 20 mL for chemical analysis. Nitrate analysis followed the ISO/DIS 15923-1 method Nitrate (NO_3^--N) was reduced to nitrite with a Cd coil to react with N-(1-naphtyl)-ethylenediamine dihydrochloride to produce a red color compound (ISO/DIS, 2013). Absorbance was measured at 546 nm. Ammonium (NH_4^+-N) was measured according to the Standard Methods 4500-NH_3 G at 660 nm of absorbance (APHA, 2005). Both measurements were done using a discrete analyzer (AQ1, Seal Analytical, Germany). For NO_3^--N and NH_4^+-N the analytical ranges were 0.01–5 and 0.001 to 1 mgL^{-1} respectively, both with ca. 5% short term repeatability.

The precipitation volume values (in grams) were used later to calculate the precipitation-weighted mean (C_{pw}) ion concentrations. Data quality control followed World Meteorological Organization (WMO) Global Atmosphere Watch (GAW) manual for the GAW precipitation chemistry programme (World Meteorological Organization, 2004) recommendations concerning laboratory data verification, reporting and acceptance criteria (see supplement material QC/QA). Simulated rainwater (ERM-CA408, European Reference Materials) was used to check methods performances. Recovery values of the ions present in the reference material ranged from 90 to 110%.

2.5. Local or distal classification criteria

Figure S1 (Supplement Materials) presents the sampling scheme and data treatment to estimate washout and rainout contributions. Figure S2 and S3 present the NO_3^--N and NH_4^+-N hourly values by season that helped identify traffic rush hour contributions. Our criteria to classify the N_r deposition as distal were:

1) the sum of event fractions had >1 mm precipitation (e.g., significant rainfall);
2) the event fractions collected in the second hour of the event were consistent; and
3) the event fractions collected outside of traffic rush hour (6–9 a.m. and 5–8pm).

The event fractions that met these criteria were considered to be distal contributions. Therefore, for these fractions, the NO_3^- and NH_4^+ as N_r concentrations were aggregated to the backward trajectories. The remainding fractions that failed to meet the above criteria were considered as local. Thus, no long distance trajectory was associated with these local event fractions.

2.6. Backward trajectories

To assess the distal origin of N_r deposition, we isolated the timings of the rain events from meteorological data and computed backward trajectories for every hour when precipitation occurred and to account for changes in synoptic weather patterns. Using Hybrid Single Particle Lagrangian Integrated Trajectory (HYSPLIT with GDAS 0.5° or GFS 0.25° input data (Stein et al., 2015)) we computed 24 h backward trajectories for each timestamp identified in a two-step process (Fleming et al., 2012): First, we used fixed endpoint heights between 500 and 4, 000 m above ground and established a linear model of their vertical levels against air temperature to interpolate the 0 °C isotherm at which we expected precipitation to form, and which we considered as "arrival levels" of incoming precipitation-forming air masses. In the second step, we incorporated a trajectory specifically for this level (Stein et al., 2015). We validated our method against radiosonde ascent data from the Hohe Warte reference observatory (available from University of Wyoming until October 2019) and we found both approaches agreed within ±10%, and which we considered as sufficient for our purposes. While the 0 °C isotherm was located <1,000 m in winter, summer heights were beyond 2,000 m and often exceeding 3000 m. We associated these trajectories with the wet-only sequentially sampled data. When there were several samples taken per hour, the trajectory closest to the sampling interval midpoint time was used. We coupled the NO_3^--N and NH_4^+-N concentrations from wet-only sequential samples with hourly backward trajectories to identify the source regions of N_r components. To minimize computational error associated with data integration, the shortest possible integration timestep was used (1 h) even though the rain event could have produced more than one sample during this time interval. In that case, each sample was aggregated to the same backward trajectory.

2.7. Data treatment

We aggregated all sample information (date/time, meteorological information, N_r chemical composition, and trajectory aggregates) into a database. As dry deposition was not collected, the bulk deposition (24 h bulk collection) was used to estimate dry deposition using:

$$Dep_{bulk} = Dep_{dry} + Dep_{wet\ only} = \sum_{i=1}^{n} C_{Bulk} \times P \quad (1)$$

where Dep_{bulk} is the bulk deposition in mg ha^{-1}, C_{Bulk} is the nitrate or ammonium concentration in mg L^{-1} (as N), measured in bulk samples in each of n rain events (n = 81), and P is the precipitation amount measured in bulk collection in mm.

Wet deposition was obtained by integration of sequentially collected data, as shown in equations (1)–(3):

$$Dep_{wet\ only} = \sum_{i=1}^{n} \sum_{j=1}^{m} C_{Seq} \times p \times 100 \quad (2)$$

where $Dep_{wet\ only}$ is the bulk wet deposition in mg ha^{-1}, C_{seq} is the nitrate or ammonium concentration in mg L^{-1} measured in each m fraction of each of n rain events sampled by the wet only sequential sampler (n = 61), p is the precipitation amount estimated by the number of tipping bucket counts registered by the sequential collector (1 tipping bucket = 0.2 mm).

$$Dep_{wet\ only}^{event\ n} = \left(\left(\sum_{i=1}^{q} C_B \times p \right)_{washout} + \left(\sum_{i=q+1}^{m} C_A \times p \right)_{rainout} \right) \times 100 \quad (3)$$

where C_A is the concentration of the N-species from the rainout. C_B is the concentration of the N-species from washout, q is the fraction when the washout process ended, and m is the total number of fractions in an individual event numbered as n.

Typically C_B and C_A correspond to the N_r concentration at the beginning and at end of the rain event respectively (Aikawa et al., 2014; Aikawa and Hiraki, 2009; Ervens, 2015; Pan et al., 2017). We considered that wet deposition contained washout and rainout contributions (eq. (3)) since washout occurs at the beginning of each rain event (fractions 1 to q) and removes gas and small particles originating from below-cloud local sources. The scavenging of distal N-sources occurs throughout the rain event but can be traced towards the end of each rain event when the local contribution is removed by washout. Therefore, the rainout process was estimated by the late fractions (q+1 up to m) of the in-cloud contribution of long-distance sources. The q fraction associated with the end of the washout was identified graphically per event when the N_r depositions were constant. The general procedure of the sampling and data treatment to estimate dry and wet deposition (washout and

rainout) is presented in Figure S1.

2.7.1. Scavenging coefficients (k) and scavenging ratios (SR)

The washout mass transfer process was expressed by a first-order reaction (eq. (4)), which allows determination of the deposition rate (in mg N L^{-1} h^{-1}) and SC (*k*, in h^{-1}) for each rain event (Ervens, 2015; Vallero, 2014; Xu et al., 2017). Half-life ($t_{1/2}$) of below-cloud N-species is the time required until the N concentration is reduced to 50% of the initial value (Novak, 1998).

$$ln\left(\frac{C_A}{C_B}\right) = -k\ .t. \therefore C_A = C_B\ .e^{-kt} \quad (4)$$

As most studies operate on 24 h or event based, the time component is not available and the SCs cannot be estimated. Therefore, we used another option that can describe the wet removal efficiency corresponds to the scavenging ratio (*SR*) calculated using eq. (5) (Pan et al., 2017):

$$SR = \frac{C_A}{C_B}.100 \quad (5)$$

Due to the high temporal resolution of sampling, the N_r concentration evolution from the start to the end of each event, the time of the day and the precipitation amount of each individual sample were used for the *k* and *SR* calculations. Later these results were compared with literature values. Rain rate variations or rain event interruptions, wind speed and direction changes were registered and associated with each sample fraction. These variations were expected to influence the washout process. For some events, the rain rate changed, and these interruptions were also considered in *k* and *SR* calculation. The Supplementary material presents C_A, C_B, *k*, *SR*, and $t_{1/2}$ calculations for all events. A one-way ANOVA was applied by season to identify statistical differences at the 0.05 confidence level.

3. Results and discussion

3.1. Precipitation coverage

Table 1 presents the completeness of rain/snow gauge measurements of precipitation depth (%PCL) at IHL-VIC and Hohe Warte meteorological stations and the completeness of precipitation depth associated with valid chemical analysis and valid sample collection (%TP), calculated in accordance with Manual for the Global Atmospheric Watch Precipitation Chemistry Programme. We compared the precipitation volumes collected to instrumental precipitation amount readings at the sampling site to nearby meteorological reference sites. The collected precipitation amounts at IHL-VIC station fell between the reported values at Hohe Warte (675 mm) and at Groß-Enzersdorf (472 mm) (Zentralanstalt für Meteorologie und Geodynamik, 2019). Wet only TP% was below the GAW acceptable annual data completeness measures when the reference station for the precipitation was Hohe Warte. However, wet only TP% fell under the acceptable annual and seasonal data completeness when IHL-VIC precipitation gauge measurements are considered.

During the period of May to December, the bulk sampler deviated ca. −20 mm from the wet-only sampler, which was attributed to a heavy 60 mm rain event in June 2019, which was not possible to capture fully due to overflow of the sampling vessel. Nonetheless, >90% of the total annual precipitation in Vienna measured at the Hohe Warte station was collected and analyzed. Other wet vs bulk discrepancies could be explained by (1) small precipitation events that did not trigger a wet-only collection and (2) the "loss" of the first bucket tip as the trigger signal for the wet-deposition sampler, which typically resulted in an under catch of 5–8% compared to the passive bulk sampler.

Table 1
Study site precipitation amount (in mm) and data completeness (in %), by time interval and by sample type for 2019.

Station	Yearly precipitation depth mm	Yearly bulk TP %	Yearly wet-only TP %	May to Dec wet only TP %
IHL-VIC	610	94.1	73.3	92.4
Hohe Warte[a]	677	90.1	66.0	88.0

[a] Values compared with Hohe Warte reference station during the same sampling interval.

3.2. Monthly concentrations of inorganic nitrogen

Mean and precipitation-amount weighted concentrations (C_{pw}) of monthly NH_4^+-N and NO_3^--N on bulk and wet-only samples and precipitation depths are presented in Fig. 2. A marked difference between the dry and wet-only N distribution was observed between spring/summer and autumn/winter. Bulk and wet depositions from May till August were similar, whereas from September till December an increase in dry deposition of NO_3^--N and NH_4^+-N was observed. This was an expected pattern typically seen in changes from wet to dry periods, as also observed by precipitation reduction from May till December.

Although in August the wet-only samples were fewer than other times of the year, they showed higher N_r concentration than the bulk samples, which yielded higher precipitation weighted concentrations of NH_4^+-N and NO_3^--N. In October, more light drizzle and fog bulk events were collected which explained the differences in C_{pw} for both species. Two bulk precipitation events yielded the highest C_{pw}. In June, the higher precipitation volumes of wet-only samples (97 mm) against bulk samples (67 mm) were attributed to intensive rain showers, which reduced the dry deposition estimate. This error propagates in the calculation of N-deposition, which is partially corrected by disregarding the sample volume and considering mass values instead. By this way, no significant amount of N species was lost nor was any sample contamination observed during the monitoring period.

3.3. Nitrogen bulk and wet-only deposition

Mean bulk NH_4^+-N and NO_3^--N deposition at the site from May–December was 13.71 ± 0.33 kg ha^{-1}. These values were higher than yearly N-depositions recorded at stations near Vienna (e.g., Lobau 4.3–6.5 kg ha^{-1} y^{-1}, from 1984 to 1999)(H Puxbaum et al., 2002). However, the data agreed with assessments that reported N throughfall between 15 and 20 kg ha^{-1} y^{-1} (NH_4^+-N + NO_3^--N) on forest and nearby open field sites (Waldner et al., 2014). The site bulk deposition values for NH_4^+-N and NO_3^--N were 8.18 ± 0.30 kg ha^{-1} and 5.34 ± 0.21 kg ha^{-1}, respectively. Ammonium (NH_4^+-N) was the predominant N form accounting for 59.6% of bulk N-deposition, which agreed with previous ranges (53–66%)(H Puxbaum et al., 2002). The wet deposition for NH_4^+-N and NO_3^--N corresponded to 79% and 70%, respectively. Similar N-depositions to our site were observed (around 7 kg ha^{-1} y^{-1}) in forested areas of Austria, but unexposed to local anthropogenic pollution emissions (Smidt, 2007, 2008). Although these studies reported NO_3^--N as the predominant N-species compared to NH_4^+-N, they confirmed highest N depositions occurred in spring (Smidt, 2008). A strong correlation between NH_4^+-N and NO_3^--N was observed in both wet and dry deposition estimates ($Dep_{NO3\text{-}N} = 0.823\ Dep_{NH4+N} + 0.11$, $R^2 = 0.921$ for wet-only and $Dep_{NO3\text{-}N} = 0.662\ Dep_{NH4+N.} + 0.015$, $R^2 = 0.863$ for dry deposition). For wet-only deposition, May and December showed significantly different NH_4^+/NO_3^- ratios, which was attributed to a reduction in NH_4^+ volatilization (Section 3.5). November, October, and December showed highest removal of NO_3^--N versus NH_4^+-N via dry deposition (See Fig. 3). In other European cities, like Kavala in Greece, NH_4^+-N is mostly removed through summer dry deposition (Beyn et al., 2014; Spanos et al., 2002). A strong correlation between NH_4^+-N and NO_3^--N in particulate matter was reported in Venice, Italy (Masiol et al., 2012), with the largest deposition amounts recorded in winter. The secondary inorganic aerosol (SIA) formation of NH_4NO_3,

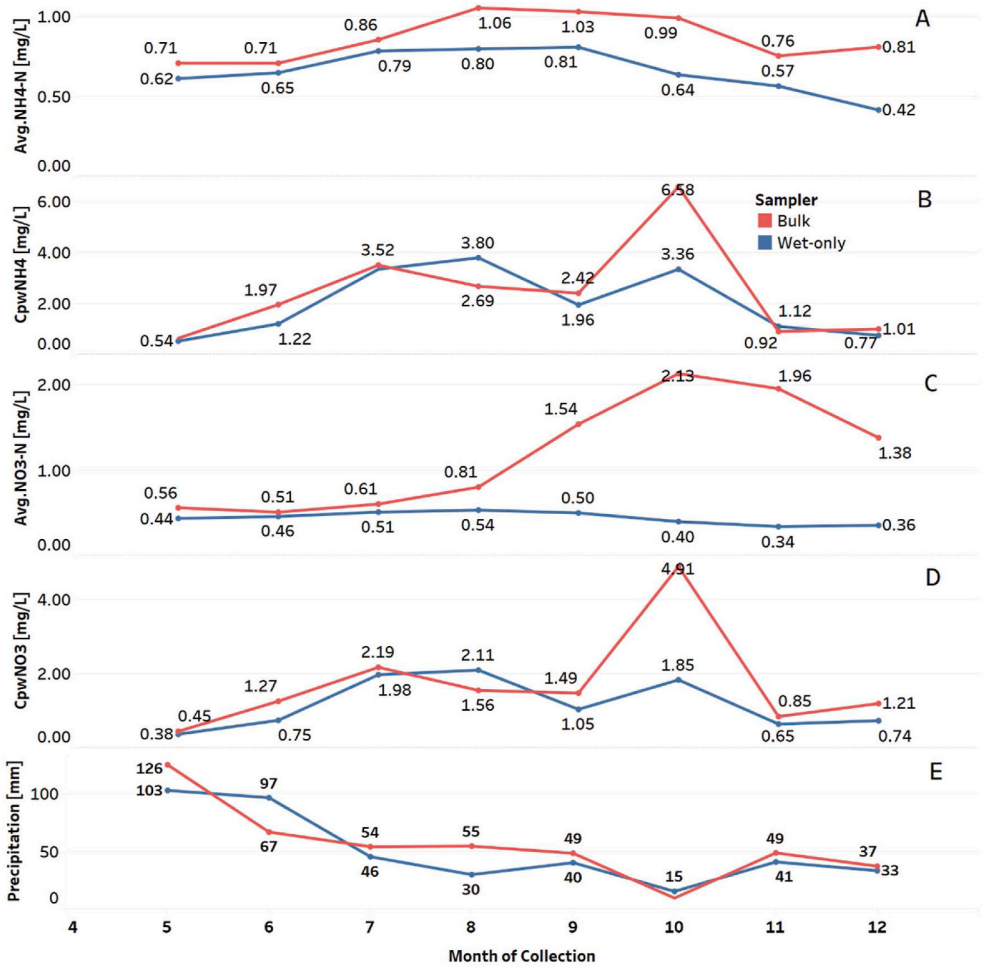

Fig. 2. Ammonium (A and B) and nitrate (C and D) concentrations in mg L^{-1}-N and precipitation amount variations (E) in bulk (in red) and wet-only (in blue) precipitation samples from May–December 2019. (For interpretation of the references to color in this figure legend, the reader is referred to the Web version of this article.)

produced by homogeneous and heterogeneous reactions increases during summer, but is quickly removed from air with larger wet deposition. In winter, the NH_4NO_3 production is reduced, but the amount produced was nearly constant under lower air temperatures and solar radiation conditions and not promptly removed by smaller precipitation (Vallero, 2014).

3.4. Evolution through a precipitation event

For both NO_3^--N and NH_4^+-N, the concentrations were higher at the beginning of the rain event or for low precipitation amounts (Fig. 4). This effect was more significant in summertime due to heavy showers with short duration. In summer and spring, the NO_3^--N and NH_4^+-N concentrations were low and constant by the end of each heavy rain event. For NO_3^--N, this was true in all seasons except for winter. At the end of the rain events, the NH_4^+-N concentration was higher in summer and spring and lower in autumn and winter, when the application of fertilizers was reduced, and temperatures were lower (Wonaschütz et al., 2015). This was attributed to strong below-cloud scavenging of airborne contaminants by first rainfall fractions (Aikawa and Hiraki, 2009; Gong et al., 2003; Xu et al., 2017). The N deposition that occurred after the first 3 mm of rain, or later were attributed to rainout only, and like results from other studies.

Long-duration rain events in the autumn and winter with constant and low rainfall rates showed distinctive oscillations in the NO_3^--N and NH_4^+-N concentrations over time (Figure S5). These oscillations were investigated by examining hourly variations of NO_3^--N and NH_4^+-N in autumn and winter (Figures S2, S3). Clear peaks in the mornings (3–9 UTC) and in the afternoons (17–21 UTC) were thereby identified. Accordingly, these peaks in concentration could be attributed to vehicle emissions during rush hour traffic. Similar hourly trends were observed for atmospheric NO_2^--N in Vienna in 2017 and 2018 (Schreier et al., 2020).

3.5. Scavenging ratios

The *SR* of NO_3^- and NH_4^+ varied among seasons from 39 to 62% and 63–69%, respectively (Table 2). When the *SR* was examined by event or fraction of events (Supplementary Material Table S1) the N-species evolution in some events showed peaks and valleys, which could not be attributed to washout or rainout processes. Therefore, we inferred those washouts could also occur during intense traffic times when the N-species concentration increases despite small precipitation amounts (lower than 0.5 mm). Pure rainout contributions were detected only in large precipitation amounts (>0.5 mm) outside of the main traffic times. Our study combines the *SR* estimation by the precipitation amount along with the high temporal resolution (Aikawa et al., 2014; Celle-Jeanton et al., 2009b; Xu et al., 2017), and allowed for clearer identification of washout and rainout contributions. Peaks and valleys in N_r were found in all seasons (Figures S2 and S3) but were particularly frequent during the wintertime. We infer that an aerosol process, with increased emissions in the lower boundary layer increases the local gas precursors

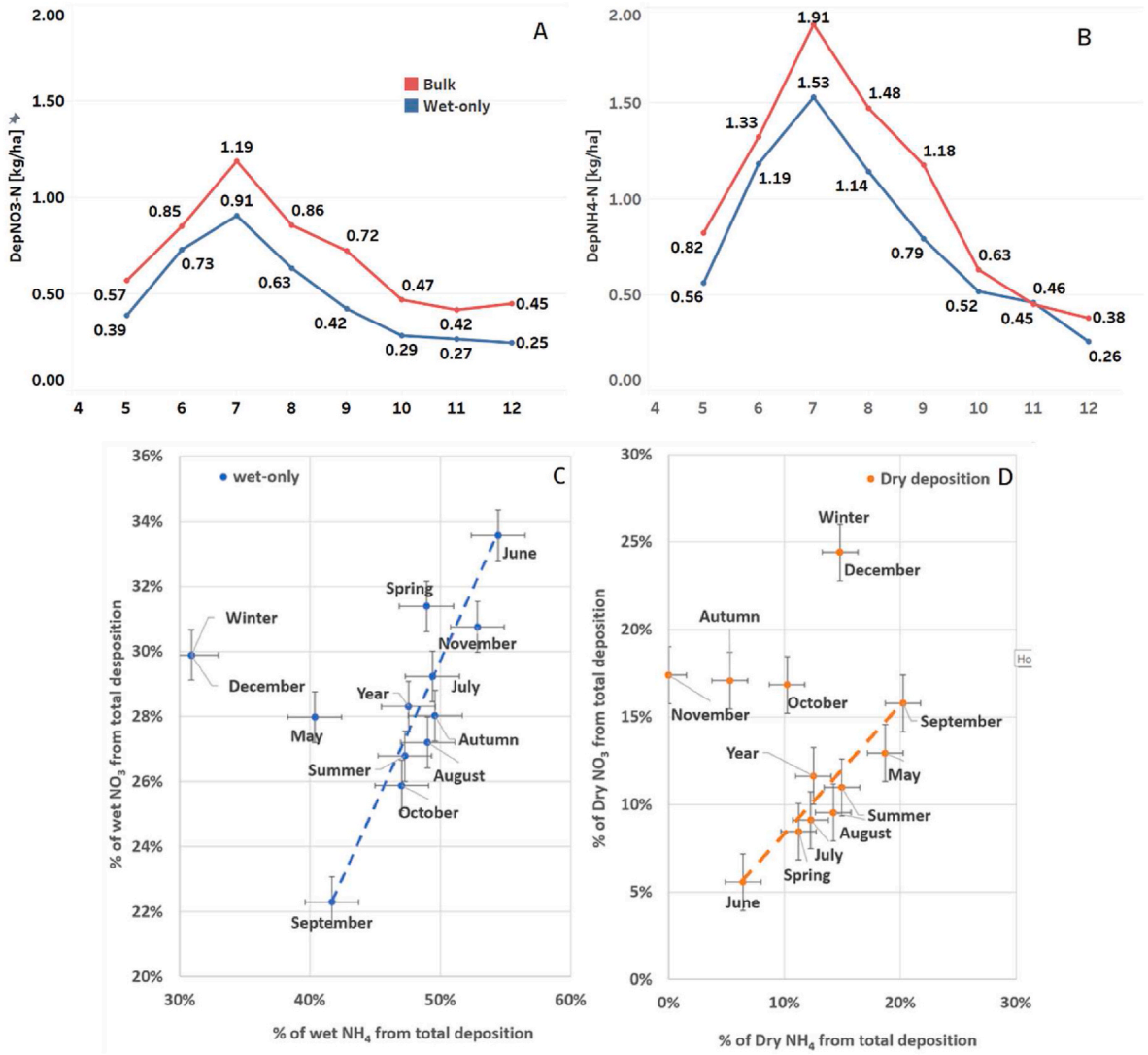

Fig. 3. Monthly variability of N-deposition (kg ha^{-1}) of (a) NO_3^--N and (b) NH_4^+-N in bulk (red) and wet-only (blue) samples and monthly contribution (%) of (c) wet-only and (d) estimated dry deposition for Vienna. Error bars indicate the uncertainties on the deposition. Dashed lines indicate correlated wet and dry deposition of NH_4^+ and NO_3^-. (For interpretation of the references to color in this figure legend, the reader is referred to the Web version of this article.)

during wintertime (Wonaschütz et al., 2015).

The usual *SR* calculations consider the initial and final conditions; however, it is well-known that this oversimplification disregards advection or changes in the air gas concentration over time and assumes a constant precipitation rate with no raindrop evaporation or change in rain droplet size (Migliavacca et al., 2010). Based on our data it seemed clear that any bias associated with the continuous supply of contaminants under the clouds cannot be corrected by using models that consider only the final and initial rainwater N_r concentrations (Xu et al., 2017). Regardless of the season, the first order modeling approximation was adequate to depict these gas-liquid effects (See supplementary material, Table S1 and Figure S6). The seasonal monitoring at high temporal resolution of a sizable number of events showed that the NH_4^+ and NO_3^- removal is kinetically different by season and is reduced during winter. This could be attributed to two factors: (a) higher summer temperatures favoring NH_4^+ volatilization and reducing its removal compared to NO_3^- and (b) lower removal efficiency to the liquid phase due the smaller precipitation amount and low cloud liquid water during winter (Kasper-Giebl et al., 2000).

The nitrate *SR* (39–62%) at our site agreed with other locations, like those in the Po Valley in Italy (40–70%)(Facchini et al., 1999; Gilardoni et al., 2014) and in Japan (60–75%) (Aikawa et al., 2014) and China (43–76%) (Xu et al., 2017). For NH_4^+-N, the *SR* (63–69%) fell within the range observed in China (30–77%) (Xu et al., 2017), and Italy (68%), but was below that reported at Puy Dome, France (86%)(Sellegri et al., 2003). In Japan, the observed reduction in the concentration of these two N-species from the beginning to the end of a rain event was associated with larger scavenging efficiency of coarse particles and water-soluble gases (Aikawa and Hiraki, 2009). In this study, the lowest *SR* values for N_r were found in wintertime, which had the lowest precipitation amount amongst the seasons. According to the Vienna City air quality monitoring, winter had the highest NO_x content (μg m^{-3}) in particulate air matter in 2019 (Spangl, 2019). This finding agrees with observations under conditions of low cloud liquid water content, under which the *SR*s are reduced (Kasper-Giebl et al., 2000) as the scavenging process requires the liquid phase to occur, and in presence of snow or ice the scavenging capability is limited.

The N_r decay after the rain started was modeled using a first order reaction. The deposition rate and half-life of the N-species were calculated by event (Supplementary Material Figure S6 and Tables S1-S2) and by season (Table 2). Both species showed the lowest and highest deposition rates in winter and summer, respectively. This was attributed to the intensity and short duration of these seasonal rain events, especially in summer, which enhanced the N-deposition rate. In general, large

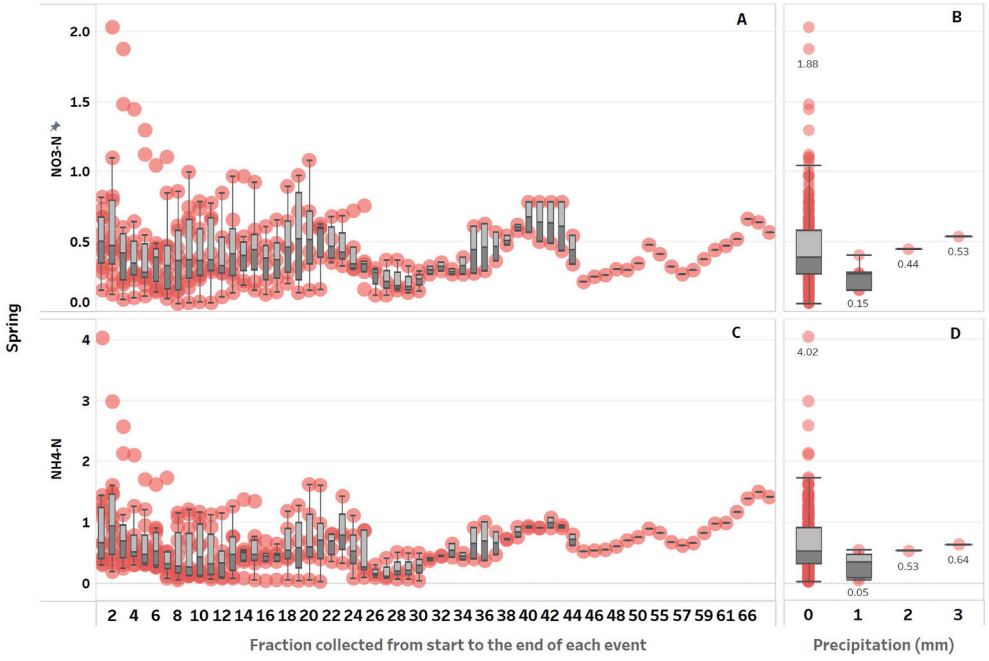

Fig. 4. Nitrate (A, B) and ammonium (C, D) (mg N L^{-1}) concentrations from the start to the end of the rain events and by precipitation amount (in mm), during the Spring 2019. For other seasons, see SM Fig. S5.

Table 2
Seasonal values of initial (C_B) and final (C_A) concentrations, scavenging ratios (SR), scavenging coefficient (k), half-life ($t_{1/2}$), and N_r rainout contribution in Vienna.

Species	Period	C_B in mg L^{-1}	C_A in mg L^{-1}	SR %	k h^{-1}	k s^{-1}	$t_{1/2}$ h	Rainout %
NO_3^--N	Spring	0.68	0.22	62	0.7	1.94×10^{-4}	1.7	38
	Summer	0.70	0.28	61	**2.9**[a]	8.06×10^{-4}	1.5	39
	Autumn	0.55	0.21	61	0.7	1.94×10^{-4}	1.9	39
	Winter	0.50	0.28	39	0.5	1.39×10^{-4}	1.6	–
	Whole season	0.63	0.24	59	1.6	4.44×10^{-4}	1.7	41
NH_4^+-N	Spring	1.03	0.34	69	0.5	1.39×10^{-4}	2.8	31
	Summer	1.15	0.47	65	1.8	5.00×10^{-4}	2.4	35
	Autumn	0.86	0.28	66	0.8	2.22×10^{-4}	2.4	34
	Winter	0.53	0.23	63	0.5	1.39×10^{-4}	1.4	–
	Whole season	0.97	0.36	65	1.1	3.06×10^{-4}	2.3	35

[a] Statistically significant difference $p = 0.03$.

variances amongst the seasons were observed for other variables (C_A, C_B, SR and $t_{1/2}$). Therefore, even with a wide range of half-lives (from 1.4 h in winter and 2.8 h in spring), no significant difference was found between seasons due to large variability within and between the rain events.

As seen in Table 2, the scavenging coefficients for NO_3^- and NH_4^+ were higher than the empirical value (8×10^{-5} s^{-1} or 0.288 h^{-1}) typically used in in-cloud wet scavenging parametrization on HYSPLIT trajectories (Stein, 2015; Tost et al., 2006; Sportisse, 2007). These empirical values were based on radionuclides (Sportisse, 2007) with no relationship to the aqueous phase chemistry of N_r species. In this study, the N_r species removal was clearly slower than the usual empirical model (Feng, 2007; Stein et al., 2015). For instance, Feng (2007) describes 73% of the coarse particles being removed in the first hour of 1–10 mm h^{-1} rain events. While in our study, the precipitation event needed to last from 1.4 to 2.8 h for a 50% reduction of N_r.

3.6. Backward trajectories

The main transport patterns identified showed long range N_r contributions coming from the NW during the spring with intermediate NO_3^--N and NH_4^+-N contributions (Fig. 5). Long-range trajectories from the W and SW during summer and W, SW and SE during the autumn had intense and intermediate contributions of NO_3^--N and NH_4^+-N, respectively. Some trajectories were consistent with studies from other parts of Central Europe and could be described as fast travelling westerly, easterly polluted, and westerly continental air masses (Okada and Hitzenberger, 2001; Wonaschütz et al., 2015). The long-range fast travelling trajectories yielded similar concentrations of NO_3^--N and NH_4^+-N like fast-travelling westerly air masses that were associated with higher concentrations of both species during summertime, but low to intermediate N concentrations during the winter.

The close-range trajectories had different concentrations of NO_3^--N and NH_4^+-N over all seasons. These trajectories showed mixed patterns during spring, with higher NO_3^--N contributions from the W and higher NH_4^+-N from all directions (N, SE, W and S). The NO_3^--N and NH_4^+-N contributions were also high in summer and autumn. The easterly trajectories had higher NH_4^+-N concentrations in all seasons. Due to the light and long-rain events in winter, no significant long or close distance air masses could be identified for that season. For wintertime, we assumed that most NO_3^--N and NH_4^+-N contributions were of local

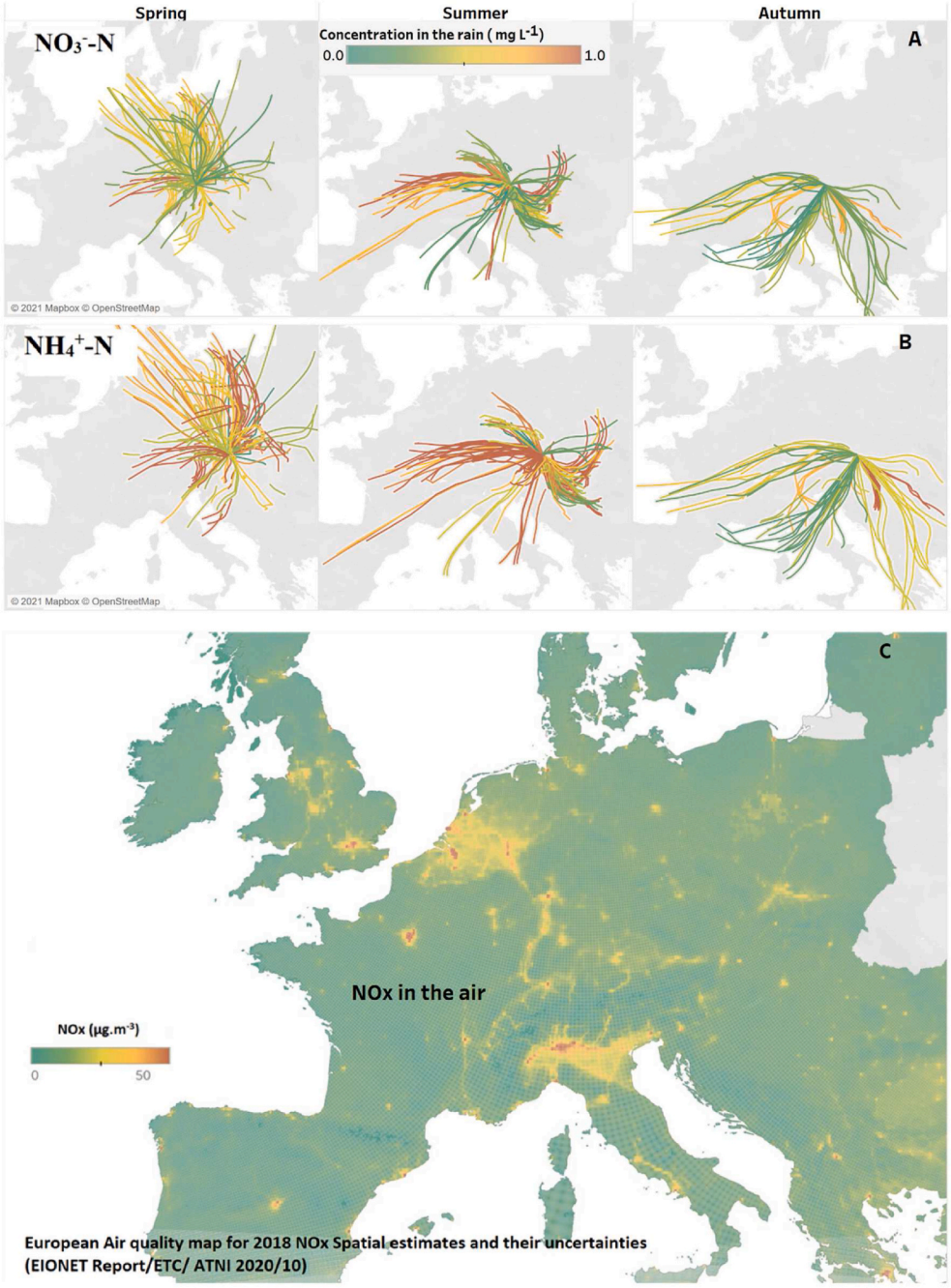

Fig. 5. Backward HYSPLIT trajectories for 2019 long-range inputs of NO_3^--N (A) and NH_4^+-N (B) in mg L^{-1} precipitation in Vienna and 2018 NO_x in the air in µg m^{-3}(C) estimates based on EIONET report (EIONET, 2021).

origin once no trajectory met the distal origin criteria.

The general understanding is that trajectories can model a source-receptor system but that may not fully represent the actual turbulent air mixing process (Stein, 2015). Several conditions can increase the trajectories uncertainties and limit their use and interpretation, such as: i)-one single trajectory may not represent accurately the NO_x origin, ii)-any event can be a mixture of several air masses, iii)- the calculated altitude of the trajectory may not represent the precipitation altitude, and vi)- some below and above cloud mixing can affect the N_r final concentration (Baldini et al., 2010). The trajectories interpretation in the present work adopted some measures to reduce these limitations and the uncertainties over the long distance source of N_r origin, such as several trajectories during different rain events among all seasons were calculated, backward and forward trajectories were calculated from the hotspots (Amsterdam, Frankfurt and Milan) to the end point of Vienna that confirmed the air mass origin, several altitudes were considered and the meteorological sonde provided a more accurate information about the 0° level and the precipitation height, and below and above cloud N_r contributions were isolated by the high frequency sampling and data processing. We believe the uncertainty regarding long distance N_r sources were reduced with these measures, even considering the usual HYSPLIT uncertainty increase with the traveled distance and mixing air masses (Baldini et al., 2010; Stein et al., 2015). The N_r trajectories were also compared to the last available NO_x EIONET air quality report (European Environment Agency, 2021) in Fig. 5c. This comparison confirmed that the HYSPLIT trajectories arriving in Vienna were from areas around Amsterdam, Frankfurt and Milan were the most probable source of long-range N_r, mainly from NW, SW, and W, respectively.

4. Conclusions

High-resolution wet-only and bulk nitrate and ammonium deposition for precipitation in Vienna was assessed to derive mass balances between bulk and wet-only samples to allow for estimates of dry and wet local and distant N_r contributions. Moreover, the rainout and washout by event and season N_r depositions were quantified and compared. The nitrate *SR* was approximately 61% for all seasons and 39% in winter. The ammonium *SR* averaged 65% for the entire year. In winter, rainout contributions to N_r were insignificant, and washout was less efficient, which explains the higher NO_x presence in wintertime. The N deposition kinetic model was a first order process, and we found a shorter half-life for nitrate (1.7 h) compared to ammonium (2.3 h). This deposition difference was attributed to higher solubility for nitrate and higher volatility for ammonium. In spring, nitrate and ammonium received significant rainout contributions from N-NW origins, whereas in summer and autumn the sources oscillated between East and Westerly sources. Wintertime had no significant long-distance N_r contribution to Vienna precipitation. These patterns matched the origin of NO_x hotspots (e.g., Amsterdam, Frankfurt, and Milan) reported for Europe. Our results suggest that seasonal high-frequency studies of N_r scavenging coefficients assessed with the drop size distribution and rain rates would help improve the empirical parametrization/modeling of in-cloud wet pollutant removal.

Availability of data and materials

The datasets used and/or analyzed during the current study are available from the corresponding author on reasonable request.

Authors' contributions

LRM and STW conceived the study, performed sample collection, chemical analysis, data compilation and interpretation, and wrote the manuscript. IM, CD and LIW participated in the conception and design of the project, performed data interpretations, and contributed to manuscript writing.

Funding

The authors received no financial support for the research, authorship, and/or publication of this article.

Declaration of competing interest

The authors declare that they have no known competing financial interests or personal relationships that could have appeared to influence the work reported in this paper.

Acknowledgements

The authors gratefully acknowledge the NOAA Air Resources Laboratory (ARL) for the provision of the HYSPLIT transport and dispersion model and READY website (https://www.ready.noaa.gov) used in this publication. We also thank the University of Wyoming's Department of Atmospheric Sciences for providing the radiosonde data, and the City of Vienna that gracefully provided the traffic and air monitoring data. We thank the anonymous reviewers for constructive comments that improved this study.

Appendix A. Supplementary data

Supplementary data to this article can be found online at https://doi.org/10.1016/j.atmosenv.2021.118740.

References

Aikawa, M., Hiraki, T., 2009. Washout/rainout contribution in wet deposition estimated by 0.5 mm precipitation sampling/analysis. Atmos. Environ. 43, 4935–4939. https://doi.org/10.1016/J.ATMOSENV.2009.07.057.

Aikawa, M., Kajino, M., Hiraki, T., Mukai, H., 2014. The contribution of site to washout and rainout: precipitation chemistry based on sample analysis from 0.5 mm precipitation increments and numerical simulation. Atmos. Environ. 95, 165–174. https://doi.org/10.1016/J.ATMOSENV.2014.06.015.

APHA, 2005. 4500-NH 3 NITROGEN (AMMONIA)* 4500-NH 3 A. Introduction.

Baldini, L.M., McDermott, F., Baldini, J.U.L., Fischer, M.J., Möllhoff, M., 2010. An investigation of the controls on Irish precipitation δ18O values on monthly and event timescales. Clim. Dynam. 35, 977–993. https://doi.org/10.1007/S00382-010-0774-6/FIGURES/6.

Beyn, F., Matthias, V., Dähnke, K., 2014. Changes in atmospheric nitrate deposition in Germany – an isotopic perspective. Environ. Pollut. 194, 1–10. https://doi.org/10.1016/J.ENVPOL.2014.06.043.

Bhattarai, H., Zhang, Y.-L., Pavuluri, C.M., Wan, X., Wu, G., Li, P., Cao, F., Zhang, W., Wang, Y., Kang, S., Ram, K., Kawamura, K., Ji, Z., Widory, D., Cong, Z., 2019. Nitrogen speciation and isotopic composition of aerosols collected at Himalayan forest (3326 m a.s.l.): seasonality, sources, and implications. Environ. Sci. Technol. 53, 12247–12256. https://doi.org/10.1021/ACS.EST.9B03999.

Celle-Jeanton, H., Travi, Y., Loÿe-Pilot, M.D., Huneau, F., Bertrand, G., 2009a. Rainwater chemistry at a Mediterranean inland station (Avignon, France): local contribution versus long-range supply. Atmos. Res. 91, 118–126. https://doi.org/10.1016/J.ATMOSRES.2008.06.003.

Celle-Jeanton, H., Travi, Y., Loÿe-Pilot, M.D., Huneau, F., Bertrand, G., 2009b. Rainwater chemistry at a Mediterranean inland station (Avignon, France): local contribution versus long-range supply. Atmos. Res. 91, 118–126. https://doi.org/10.1016/j.atmosres.2008.06.003.

Chen, Z., Liu, C., Liu, W., Zhang, T., Xu, J., 2017. A synchronous observation of enhanced aerosol and NO2 over Beijing, China, in winter 2015. Sci. Total Environ. 575, 429–436. https://doi.org/10.1016/J.SCITOTENV.2016.09.189.

Cheng, I., Zhang, L., 2016. Long-term air concentrations, wet deposition, and scavenging ratios of inorganic ions, HNO_3 and SO_2 and assessment of aerosol and precipitation acidity at Canadian rural locations. Atmos. Chem. Phys. Discuss. 1–42. https://doi.org/10.5194/ACP-2016-918.

Ciężka, M., Modelska, M., Górka, M., Trojanowska-Olichwer, A., Widory, D., 2016. Chemical and isotopic interpretation of major ion compositions from precipitation: a one-year temporal monitoring study in Wrocław, SW Poland. J. Atmos. Chem. 73, 61–80. https://doi.org/10.1007/s10874-015-9316-2.

City of Vienna, 2019. Luftqualität der Stadt Wien - Monats- und Jahresberichte. Vienna.

City of Vienna, 2016. Straßenverkehrszählung wien 2015 [WWW Document]. URL. https://www.wien.gv.at/stadtentwicklung/studien/pdf/b008495.pdf. accessed 8.26.21.

Coplen, T.B., Neiman, P.J., White, A.B., Ralph, F.M., 2015. Categorisation of northern California rainfall for periods with and without a radar brightband using stable isotopes and a novel automated precipitation collector†. https://doi.org/10.3402/tellusb.v67.28574 6.28574. https://doi.org/10.3402/TELLUSB.V67.28574.

Ervens, B., 2015. Modeling the processing of aerosol and trace gases in clouds and fogs. Chem. Rev. 115, 4157–4198. https://doi.org/10.1021/CR5005887.

European Environment Agency, 2021. Interpolated air quality data from 2018 [WWW Document]. URL. https://www.eea.europa.eu/data-and-maps/data/interpolated-air-quality-data-2. accessed 8.26.21.

Facchini, M.C., Fuzzi, S., Zappoli, S., Andracchio, A., Gelencsér, A., Kiss, G., Krivácsy, Z., Mészáros, E., Hansson, H.-C., Alsberg, T., Zebühr, Y., 1999. Partitioning of the organic aerosol component between fog droplets and interstitial air. J. Geophys. Res. Atmos. 104, 26821–26832. https://doi.org/10.1029/1999JD900349.

Feng, J., 2007. A 3-mode parameterization of below-cloud scavenging of aerosols for use in atmospheric dispersion models. Atmos. Environ. 41, 6808–6822. https://doi.org/10.1016/J.ATMOSENV.2007.04.046.

Feng, J., Vet, R., Cole, A., Zhang, L., Cheng, I., O'Brien, J., Macdonald, A.M., 2021. Inorganic chemical components in precipitation in the eastern U.S. and Eastern Canada during 1989–2016: temporal and regional trends of wet concentration and wet deposition from the NADP and CAPMoN measurements. Atmos. Environ. 254, 118367. https://doi.org/10.1016/J.ATMOSENV.2021.118367.

Fleming, Z.L., Monks, P.S., Manning, A.J., 2012. Review: untangling the influence of air-mass history in interpreting observed atmospheric composition. Atmos. Res. 104–105, 1–39. https://doi.org/10.1016/J.ATMOSRES.2011.09.009.

Gilardoni, S., Massoli, P., Giulianelli, L., Rinaldi, M., Paglione, M., Pollini, F., Lanconelli, C., Poluzzi, V., Carbone, S., Hillamo, R., Russell, L.M., Facchini, M.C., Fuzzi, S., 2014. Fog scavenging of organic and inorganic aerosol in the po valley. Atmos. Chem. Phys. 14, 6967–6981. https://doi.org/10.5194/ACP-14-6967-2014.

Gong, S.L., Barrie, L.A., Blanchet, J.-P., Salzen, K. von, Lohmann, U., Lesins, G., Spacek, L., Zhang, L.M., Girard, E., Lin, H., Leaitch, R., Leighton, H., Chylek, P., Huang, P., 2003. Canadian Aerosol Module: a size-segregated simulation of atmospheric aerosol processes for climate and air quality models 1. Module development. J. Geophys. Res. Atmos. 108 https://doi.org/10.1029/2001JD002002. AAC 3-1.

Holtgrieve, G.W., Schindler, D.E., Hobbs, W.O., Leavitt, P.R., Ward, E.J., Bunting, L., Chen, G., Finney, B.P., Gregory-Eaves, I., Holmgren, S., Lisac, M.J., Lisi, P.J., Nydick, K., Rogers, L.A., Saros, J.E., Selbie, D.T., Shapley, M.D., Walsh, P.B., Wolfe, A.P., 2011. A coherent signature of anthropogenic nitrogen deposition to remote watersheds of the Northern Hemisphere. Science (80) 334, 1545–1548. https://doi.org/10.1126/science.1212267.

ISO/DIS, 2013. ISO 15923-1:2013 - water quality — determination of selected parameters by discrete analysis systems — Part 1: ammonium, nitrate, nitrite, chloride, orthophosphate, sulfate and silicate with photometric detection [WWW Document]. URL. https://www.iso.org/standard/55559.html. accessed 8.27.21.

Karadeniz, H., Yenisoy-Karakaş, S., 2020. Evaluation of hourly-based precipitation chemistry in suburban site of Bolu. Atmos. Pollut. Res. 11, 2164–2172. https://doi.org/10.1016/J.APR.2020.06.023.

Kasper-Giebl, A., Koch, A., Hitzenberger, R., Puxbaum, H., 2000. Scavenging efficiency of 'aerosol carbon' and sulfate in supercooled clouds at Mt. Sonnblick (3106 m a.s.l., Austria). J. Atmos. Chem. 351 (35), 33–46. https://doi.org/10.1023/A:1006250508562, 2000.

Keene, W.C., Galloway, J.N., Likens, G.E., Deviney, F.A., Mikkelsen, K.N., Moody, J.L., Maben, J.R., 2015. Atmospheric wet deposition in remote regions: benchmarks for environmental change. J. Atmos. Sci. 72, 2947–2978. https://doi.org/10.1175/JAS-D-14-0378.1.

Laakso, L., Grönholm, T., Rannik, Ü., Kosmale, M., Fiedler, V., Vehkamäki, H., Kulmala, M., 2003. Ultrafine particle scavenging coefficients calculated from 6 years field measurements. Atmos. Environ. 37, 3605–3613. https://doi.org/10.1016/S1352-2310(03)00326-1.

Leder, K., Puxbaum, H., Kreiner, P., Tarmann, V., 2003. NASSE DEPOSITION IM LAND WIEN OKTOBER 02-SEPTEMBER 03. TUV CTA LEA.

Lee, D.S., Kingdon, R.D., Jenkin, M.E., Garland, J.A., 2000. Modelling the atmospheric oxidised and reduced nitrogen budgets for the UK with a Lagrangian multi-layer long-range transport model. Environ. Model. Assess. 5.

Li, C., Li, S.L., Yue, F.J., He, S.N., Shi, Z.B., Di, C.L., Liu, C.Q., 2020. Nitrate sources and formation of rainwater constrained by dual isotopes in Southeast Asia: example from Singapore. Chemosphere 241, 125024. https://doi.org/10.1016/J.CHEMOSPHERE.2019.125024.

Li, Y., Schichtel, B.A., Walker, J.T., Schwede, D.B., Chen, X., Lehmann, C.M.B., Puchalski, M.A., Gay, D.A., Collett, J.L., 2016. Increasing Importance of Deposition of Reduced Nitrogen in the United States 113. https://doi.org/10.1073/pnas.1525736113.

Malagó, A., Bouraoui, F., 2021. Global anthropogenic and natural nutrient fluxes: from local to planetary assessments. Environ. Res. Lett. 16, 054074 https://doi.org/10.1088/1748-9326/ABE95F.

Masiol, M., Squizzato, S., Ceccato, D., Rampazzo, G., Pavoni, B., 2012. Determining the influence of different atmospheric circulation patterns on PM10 chemical composition in a source apportionment study. Atmos. Environ. 63, 117–124. https://doi.org/10.1016/J.ATMOSENV.2012.09.025.

Matiatos, I., Wassenaar, L.I., Monteiro, L.R., Terzer-Wassmuth, S., Douence, C., 2021. Isotopic Composition (δ15N, δ18O) of Nitrate in High-Frequency Precipitation Events Differentiate Atmospheric Prossesse and Anthropogenic NOx Emissions (under review).

Michelsen, N., van Geldern, R., Roßmann, Y., Bauer, I., Schulz, S., Barth, J.A.C., Schüth, C., 2018. Comparison of precipitation collectors used in isotope hydrology. Chem. Geol. 488, 171–179. https://doi.org/10.1016/j.chemgeo.2018.04.032.

Migliavacca, D.M., Teixeira, E.C., Rodriguez, M.T.R., Wiegand, F., Pereira, F.N., 2010. Analysis of the sulfate aerosol scavenging processes in the metropolitan area of Porto Alegre (MAPA), RS, Brazil. Atmos. Pollut. Res. 1, 82–93. https://doi.org/10.5094/APR.2010.011.

Montoya-Mayor, R., Fernández-Espinosa, A.J., Ternero-Rodríguez, M., 2011. Assessment of the sequential principal component analysis chemometric tool to identify the soluble atmospheric pollutants in rainwater. Anal. Bioanal. Chem. 399, 2031–2041. https://doi.org/10.1007/s00216-010-4371-7.

Novak, I., 1998. Chemical kinetics without calculus. J. Chem. Educ. 75, 1574. https://doi.org/10.1021/ED075P1574.

Okada, K., Hitzenberger, R.M., 2001. Mixing properties of individual submicrometer aerosol particles in Vienna. Atmos. Environ. 35, 5617–5628. https://doi.org/10.1016/S1352-2310(01)00126-1.

Pan, Y.-P., Zhu, X.-Y., Tian, S.-L., Wang, L.-L., Zhang, G.-Z., Zhou, Y.-B., Xu, P., Hu, B., Wang, Y.-S., 2017. Wet deposition and scavenging ratio of air pollutants during an extreme rainstorm in the North China Plain. New pub KeAi 10, 348–353. https://doi.org/10.1080/16742834.2017.1343084.

Porfírio, D.M., Monteiro, L.R., da Costa, M.L., 2020. Rainwater geochemistry inside the Barcarena power station at the mouth of the Tocantins River. Environ. Technol. (United Kingdom) 41, 981–996. https://doi.org/10.1080/09593330.2018.1516801.

Puxbaum, H., Simeonov, V., Kalina, M., Tsakovski, S., Löffler, H., Heimburger, Biebl, P., Weber, A., Damm, A., 2002. Long-term assessment of the wet precipitation chemistry in Austria (1984-1999). Chemosphere 48, 733–747. https://doi.org/10.1016/S0045-6535(02)00125-X.

Reis, S., Pinder, R.W., Zhang, M., Lijie, G., Sutton, M.A., 2009. Reactive nitrogen in atmospheric emission inventories. Atmos. Chem. Phys. 9, 7657–7677. https://doi.org/10.5194/acp-9-7657-2009.

Roy, A., Chatterjee, A., Ghosh, A., Das, S.K., Ghosh, S.K., Raha, S., 2019. Below-cloud scavenging of size-segregated aerosols and its effect on rainwater acidity and nutrient deposition: a long-term (2009–2018) and real-time observation over eastern Himalaya. Sci. Total Environ. 674, 223–233. https://doi.org/10.1016/J.SCITOTENV.2019.04.165.

Schreier, S.F., Richter, A., Peters, E., Ostendorf, M., Schmalwieser, A.W., Weihs, P., Burrows, J.P., 2020. Dual ground-based MAX-DOAS observations in Vienna, Austria: evaluation of horizontal and temporal NO2, HCHO, and CHOCHO distributions and comparison with independent data sets. Atmos. Environ. X 5, 100059. https://doi.org/10.1016/J.AEAOA.2019.100059.

Sellegri, K., Laj, P., Dupuy, R., Legrand, M., Preunkert, S., Putaud, J.-P., 2003. Size-dependent scavenging efficiencies of multicomponent atmospheric aerosols in clouds. J. Geophys. Res. Atmos. 108, 4334. https://doi.org/10.1029/2002JD002749.

Smidt, S., 2008. Depositionsmessungen auf den Level II-Flächen 1996-2007. FORSTSCHUTZ AKTUELL 43, 37.

Smidt, S., 2007. Immissionsbelastung durch nasse Niederschläge auf den Level II-Flächen. FORSTSCHUTZ AKTUELL 38.

Spangl, W., 2019. Luftgütemessungen und meteorologische Messungen (Wien).

Spanos, T., Simeonov, V., Andreev, G., 2002. Environmetric modeling of emission sources for dry and wet precipitation from an urban area. Talanta 58, 367–375. https://doi.org/10.1016/S0039-9140(02)00285-0.

Sportisse, B., 2007. A review of parameterizations for modelling dry deposition and scavenging of radionuclides. Atmos. Environ. 41, 2683–2698. https://doi.org/10.1016/J.ATMOSENV.2006.11.057.

Sportisse, B., Bois, L. du, 2002. Numerical and theoretical investigation of a simplified model for the parameterization of below-cloud scavenging by falling raindrops. Atmos. Environ. 36, 5719–5727. https://doi.org/10.1016/S1352-2310(02)00576-9.

Stadt Wien, 2020. Jahresbericht 2019 - Luftgütemessungen der Umweltschutzabteilung der Stadt Wien.

Stein, A.F., Draxler, R.R., Rolph, G.D., Stunder, B.J.B., Cohen, M.D., Ngan, F., 2015. NOAA's HYSPLIT atmospheric transport and dispersion modeling system. Bull. Am. Meteorol. Soc. 96, 2059–2077. https://doi.org/10.1175/BAMS-D-14-00110.1.

Stevenazzi, S., Camera, C.A.S., Masetti, M., Azzoni, R.S., Ferrari, E.S., Tiepolo, M., 2020. Atmospheric nitrogen depositions in a highly human-impacted area. Water, Air, Soil Pollut. 2316 (231), 1–19. https://doi.org/10.1007/S11270-020-04613-Y, 2020.

Tost, H., Jöckel, P., Kerkweg, A., Sander, R., Lelieveld, J., 2006. Technical note: a new comprehensive SCAVenging submodel for global atmospheric chemistry modelling. Atmos. Chem. Phys. 6, 565–574. https://doi.org/10.5194/ACP-6-565-2006.

UNEP, 2007. Too Much or Too Little of a Good Thing.

Vallero, D.A., 2014. Fundamentals of Air Pollution. Elsevier Science.

Vet, R., Artz, R.S., Carou, S., Shaw, M., Ro, C.U., Aas, W., Baker, A., Bowersox, V.C., Dentener, F., Galy-Lacaux, C., Hou, A., Pienaar, J.J., Gillett, R., Forti, M.C., Gromov, S., Hara, H., Khodzher, T., Mahowald, N.M., Nickovic, S., Rao, P.S.P., Reid, N.W., 2014. A global assessment of precipitation chemistry and deposition of sulfur, nitrogen, sea salt, base cations, organic acids, acidity and pH, and phosphorus. Atmos. Environ. 93, 3–100. https://doi.org/10.1016/J.ATMOSENV.2013.10.060.

Villalobos-Forbes, M., Esquivel-Hernández, G., Sánchez-Murillo, R., Sánchez-Gutiérrez, R., Matiatos, I., 2021. Stable isotopic characterization of nitrate wet deposition in the tropical urban atmosphere of Costa Rica. Environ. Sci. Pollut. Res. 1–16. https://doi.org/10.1007/S11356-021-15327-X, 2021.

Vizcaino, P., Lavalle, C., 2018. Development of European NO2 Land Use Regression Model for present and future exposure assessment: implications for policy analysis. Environ. Pollut. 240, 140–154. https://doi.org/10.1016/J.ENVPOL.2018.03.075.

Waldner, P., Marchetto, A., Thimonier, A., Schmitt, M., Rogora, M., Granke, O., Mues, V., Hansen, K., Pihl Karlsson, G., Žlindra, D., Clarke, N., Verstraeten, A., Lazdins, A., Schimming, C., Iacoban, C., Lindroos, A.J., Vanguelova, E., Benham, S., Meesenburg, H., Nicolas, M., Kowalska, A., Apuhtin, V., Napa, U., Lachmanová, Z., Kristoefel, F., Bleeker, A., Ingerslev, M., Vesterdal, L., Molina, J., Fischer, U., Seidling, W., Jonard, M., O'Dea, P., Johnson, J., Fischer, R., Lorenz, M., 2014. Detection of temporal trends in atmospheric deposition of inorganic nitrogen and sulphate to forests in Europe. Atmos. Environ. 95, 363–374. https://doi.org/10.1016/J.ATMOSENV.2014.06.054.

Wen, Z., Xu, W., Li, Q., Han, M., Tang, A., Zhang, Y., Luo, X., Shen, J., Wang, W., Li, K., Pan, Y., Zhang, L., Li, W., Collett, J.L., Zhong, B., Wang, X., Goulding, K., Zhang, F., Liu, X., 2020. Changes of nitrogen deposition in China from 1980 to 2018. Environ. Int. 144, 106022. https://doi.org/10.1016/J.ENVINT.2020.106022.

Wien Energie, 2018. Umweltkennzahlen gesamt – Wien Energie Umwelt [WWW Document]. URL. https://pagestrip.com/de/wien-energie-umwelt-2018/8QgId5IG/umweltkennzahlen-gesamt/. accessed 8.26.21.

Wonaschütz, A., Demattio, A., Wagner, R., Burkart, J., Zíková, N., Vodička, P., Ludwig, W., Steiner, G., Schwarz, J., Hitzenberger, R., 2015. Seasonality of new particle formation in Vienna, Austria – influence of air mass origin and aerosol chemical composition. Atmos. Environ. 118, 118–126. https://doi.org/10.1016/J.ATMOSENV.2015.07.035.

World Meteorological Organization, 2004. WORLD METEOROLOGICAL ORGANIZATION GLOBAL ATMOSPHERE WATCH No. 160 MANUAL for the GAW PRECIPITATION CHEMISTRY PROGRAMME Guidelines, Data Quality Objectives and Standard Operating Procedures.

Xiao, J., 2016. Chemical composition and source identification of rainwater constituents at an urban site in Xi'an. Environ. Earth Sci. 75 https://doi.org/10.1007/s12665-015-4997-z.

Xu, D., Ge, B., Wang, Z., Sun, Y., Chen, Y., Ji, D., Yang, T., Ma, Z., Cheng, N., Hao, J., X, Y., 2017. Below-cloud wet scavenging of soluble inorganic ions by rain in Beijing during the summer of 2014. Environ. Pollut. 230, 963–973. https://doi.org/10.1016/J.ENVPOL.2017.07.033.

Ye, X., Tao, Y., Liu, Y., Wang, R., Li, Q., Yang, X., Chen, J., 2019. Size-fractionated water-soluble ions during autumn and winter: insights into volatile ammonium formation mechanisms in Shanghai, a megacity of China. Atmos. Environ. X 2, 100011. https://doi.org/10.1016/J.AEAOA.2019.100011.

Zentralanstalt für Meteorologie und Geodynamik, 2019. Klimamonitoring — ZAMG [WWW Document]. URL. https://www.zamg.ac.at/cms/de/klima/klima-aktuell/klimamonitoring/?station=5904&param=rr&period=period-y-2019&ref=3. accessed 8.26.21.

Zhang, Y., Xu, W., Wen, Z., Wang, D., Hao, T., Tang, A., Liu, X., 2017. Atmospheric deposition of inorganic nitrogen in a semi-arid grassland of Inner Mongolia, China. J. Arid Land 9, 810–822. https://doi.org/10.1007/s40333-017-0071-x.